11th International Workshop on Ship and Marine Hydrodynamics
Hamburg, Germany, September 22-25, 2019

RANS Model for Bow Wave Breaking of a KRISO Container Ship under Different Speeds

Anzheng Yu, Decheng Wan*

State Key Laboratory of Ocean Engineering, School of Naval Architecture, Ocean and Civil Engineering Shanghai Jiao Tong University, Collaborative Innovation Center for Advanced Ship and Deep-Sea Exploration, Shanghai, China

*Corresponding Author: dcwan@sjtu.edu.cn

ABSTRACT

RANS model combined with VOF method is used to simulate the bow wave breaking of KCS model in the present work. Numerical simulations under seven Froude numbers are conducted in our inhouse CFD solver naoe-FOAM-SJTU. The results of total resistance coefficient and wave pattern at Fr=0.26 are used for CFD validation. The results of resistance coefficients and wave surface on ship hull under different Froude numbers are analysed, the overall results show that present numerical methods can deal with the complex flow around ship model. Comparisons of bow wave between model test and CFD at Fr=0.26, 0.35, 0.425 are given, the vorticities induced by bow wave breaking is also analysed. In order to figure out the mechanism of bow wave breaking, detail analysis of wave cuts is provided at Fr=0.35, both plunging and spilling wave-breaking are found as well as air-entertainment and splash. Present RANS model can accurately capture the overturning of bow wave but cannot deal with the unsteady capillary wave which is found in model test.

1 INTRODUCTION

Ship bow wave breaking has been investigated for a long time since its specific impact on ship performance is still unknown. Wave breaking is an unsteady and strong-nonlinearity phenomenon which means a challenge for computational fluid dynamics (CFD), furthermore, the simulation of wave breaking has been chosen as one of the benchmarks of CFD 2021 Workshop.

Limited by the development of computer devices and technology, the past studies about breaking waves were usually conducted by experimental fluid dynamics (EFD) and theoretical derivation. Baba discovered the breaking wave resistance through physical experiment and theoretical analysis [1]. Duncan measured the wave height profile and the velocity field of a two-dimensional hydrofoil and found that the drag related with the breaking zone is more than three times the drag of the non-breaking hypothetical situation obtained by theory. The author also found that the wave breaking is more likely to happen when the wave slop is higher than 17° [2]. Dong et al. studied the vorticity induced by ship bow wave through Particle Image Velocimetry (PIV) and free-surface visualizations [3]. A two-dimensional plunging wave-breaking test was conducted by Kang et al. [4], the process of breaking and small scaled characteristics (vortex and air tube) were discussed. Olivieri et al. studied the scars and vortices induced by bow and shoulder wave breaking of a David-Taylor model basin Model 5415 (DTMB5415) and the effects of Froude number and scale ratio was considered [5].

CFD is a useful tool to get details of the flow and figure out the breaking mechanism. The Reynolds-averaged Navier-Stokes (RANS) model is widely used in numerical simulation of wave breaking. In early studies, Rhee S. H and Stern F predicted the spilling breaking wave through this model [6]. Wilson et al. combined the RANS model with the level set method to deal with the bow wave breaking of DTMB5414 model [7]. The results of CFD show good agreement with experimental data in Olivieri's work [5]. Wang et al. [8] and Ren et al. [9] simulated the bow wave breaking by in-house CFD solver naoe-FOAM-SJTU [10]. The results of resistance, wave elevations and flow velocities show that the solver can accurately predict the

breaking of bow wave. Marrone et al. applied the Smoothed Particle Hydrodynamics (SPH) method to simulating the wave pattern and bow wave breaking of a slender ship [11][12].

Present work is based on the model test conducted by Towing Tank at Shanghai Jiao Tong University and focus on the bow wave breaking of a KRISO Container Ship (KCS) advancing in calm water. In-house CFD solver naoe-FOAM-SJTU is employed for numerical simulation and detail information of bow wave region is given. The numerical method is stated in the second where the third part gives the information of ship geometry and test conditions. Then comes the mesh distribution and validation, the details of mesh generation are given. The fifth part are numerical results and analysis, the comparisons of bow wave between CFD and EFD at Fr=0.26, Fr=0.35 and Fr=0.425 are provided and the vorticities induced by bow wave are analysed. Besides, detail analysis is conducted at Fr=0.35 and air-entertainment, bow wave overturning can be found.

2 NUMERICAL METHOD

Present work is conducted by the ship hydrodynamics CFD solver, naoe-FOAM-SJTU. RANS model combined with Volume of Fluid (VOF) method is used to investigate the bow wave breaking under different speeds. The blended k-ε, k-ω shear stress transport (SST) turbulence model is applied to simulate the turbulent flow. The computational domain is discretized by hexahedral unstructured grid generated by HEXPRESS and the finite volume method (FVM) is used to transform RANS and VOF equations into computational space. The PISO-SIMPLE (PIMPLE) algorithm is used to solving the pressure-velocity coupling equations.

2.1 Governing equations

The incompressible RANS equations can be expressed as a mass conservation equation and a momentum conservation equation:

$$\nabla \cdot \boldsymbol{U} = 0 \tag{1}$$

$$\frac{\partial(\rho \boldsymbol{U})}{\partial t} + \nabla \cdot \left(\rho\left(\boldsymbol{U} - \boldsymbol{U}_g\right)\boldsymbol{U}\right) = -\nabla p_d - g \cdot x \nabla \rho + \nabla \cdot \left(\mu_{eff} \nabla \boldsymbol{U}\right) + (\nabla \boldsymbol{U}) \cdot \nabla \mu_{eff} + f_\sigma \tag{2}$$

where $\boldsymbol{U}$ is fluid velocity and $\boldsymbol{U}_g$ is the grid velocity; p_d is the dynamic pressure and ρ means the mixture density; g represents the gravity acceleration; μ_{eff} is the effective dynamic viscosity and can be written as $\rho(\nu+\nu_t)$, in which ν is the kinetic viscosity where ν_t is the eddy viscosity. f_σ is the surface tension term.

2.2 VOF method

The VOF method in OpenFOAM with bounded artificial compression is applied to capture the air-water surface.

$$\frac{\partial \alpha}{\partial t} + \nabla \cdot \left(\rho\left(\boldsymbol{U} - \boldsymbol{U}_g\right)\alpha\right) + \nabla \cdot \left(\boldsymbol{U}_r\left(1-\alpha\right)\alpha\right) = 0 \tag{3}$$

where α is the volume fraction, means the relative proportion of fluid in each grid. 0 represents air phase and 1 means water phase whereas $0<\alpha<1$ stands for the air-water interface:

$$\begin{cases} \alpha = 0 & \text{air} \\ 0 < \alpha < 1 & \text{interface} \\ \alpha = 1 & \text{water} \end{cases} \tag{4}$$

In Eq. (3), $\boldsymbol{U}_r$ means the velocity field employed to compress the two-phase surface, and it only works on the interface where $(1-\alpha)\alpha$ is not equal to zero.

3 GEOMETRY AND CONDITIONS

3.1 Geometry

In present study, a 6m-long KCS model with rudder is selected and the three-dimensional view is shown in Figure1. The main particulars in design draft are listed in Table 1 and the scale ratio here is 37.89. Video and photo study were carried out by Towing Tank at Shanghai Jiao Tong University under 7 Froude numbers (Fr=0.26, 0.30, 0.325, 0.35, 0.375, 0.40 and 0.425) in order to investigate the influence of speeds on wave breaking.

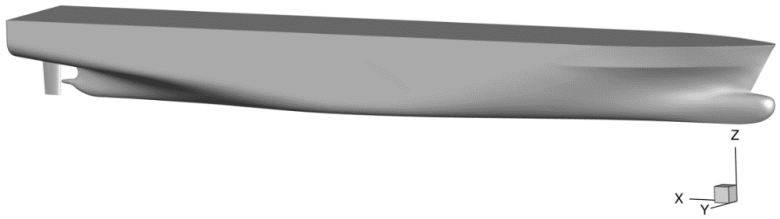

Figure 1: Three-dimensional model of KCS

Table 1: Main Particulars of KCS

Main Particulars		Full scale	Present Model
Scale ratio	——	——	37.89
Length between perpendiculars	L_{PP} (m)	230	6.0702
Beam of waterline	B_{WL}(m)	32.2	0.8498
Depth	D (m)	19.0	0.5015
Draft	T (m)	10.8	0.2850
Displacement volume	∇ (m^3)	52030	0.9571
Wetted surface area with rudder	S (m^2)	9539	6.6978

3.2 Test Conditions

The numerical simulation follows the model test and seven Froude numbers are taken into account to study the bow wave breaking. The water density is set to 998.63 kg/m^3 and the gravity acceleration is 9.81 m/s^2. The coefficient of kinematic viscosity is 1.14×10^{-6} m^2/s. Besides, the heave and pitch motions are fixed in the initial state (design draft) during the simulation in order to reduce the impact of ship motions on wave breaking

4 GRID DISTRIBUTION AND VALIDATION

4.1 Grid distribution

The computational domain is shown in Figure 2. In present work, the origin of the coordinates is set at the intersection of ship bow and waterline. The x-axis points to ship stern and the direction of y-axis is positive to starboard whereas z-axis is up positive. As shown in Figure 2, the domain range is: $-1.0L_{PP}<x<4.0L_{PP}$, $0<y<1.5L_{PP}$, $-1.0LPP<z<0.75L_{PP}$.

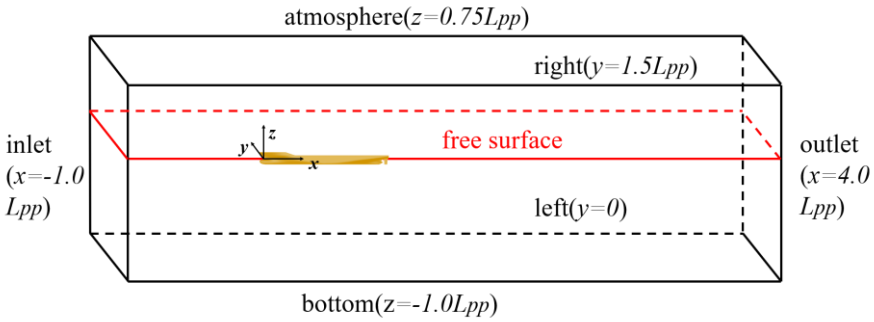

Figure 2: Computation domain and coordinate axis setting

Unstructured hexahedral grids are generated by HEXPRESS and the total grid number are 6.7M. Figure3(a) shows the overview of grid generation and the number of initial grids is $80\times24\times36$ in three directions. The size of girds around the free surface is refined 1/8 of the background grids to capture the interface. In order to simulate the bow wave and capture the small scale characters, four refinement boxes are set as shown in Figure 3(b) and the grid size are 1/2, 1/8, 1/16, 1/32 of the initial grid, respectively.

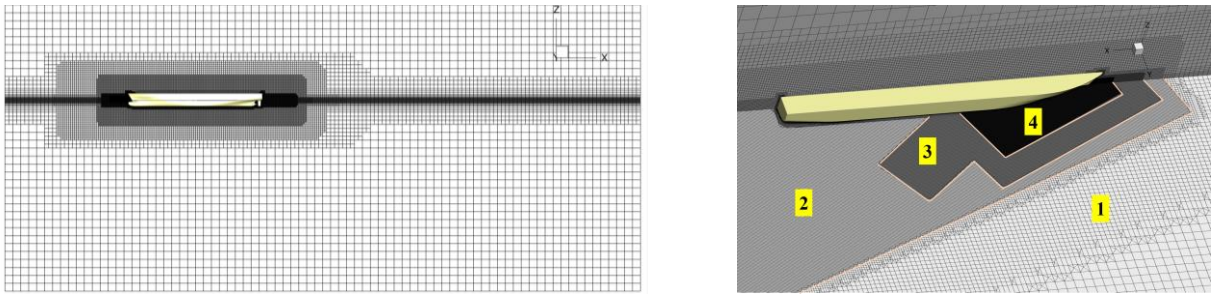

(a) Overview of mesh generation (b) Mesh refinement regions

Figure 3: Mesh distribution and refinement regions set

4.2 Grid validation

The wave pattern and the total resistance coefficient C_t at Fr=0.26 are employed for CFD validation. In present work, C_t is 3.724×10^{-3} where EFD of C_t is 3.835×10^{-3} and the error is 2.89%. Considering that the model test is free to pitch and heave, the error is acceptable. The comparison of free surface wave pattern between present work and EFD data is shown in Figure 4. The results are in good agreement with the test and distinct Kelvin angle can be observed in the wave system. Besides, both the divergent and transverse wave components show good agreement with EFD data. Present numerical simulations are carried out in calm water and the above results are all in good agreement with model test data, indicating that present numerical methods can accurately deal with the flow around KCS model.

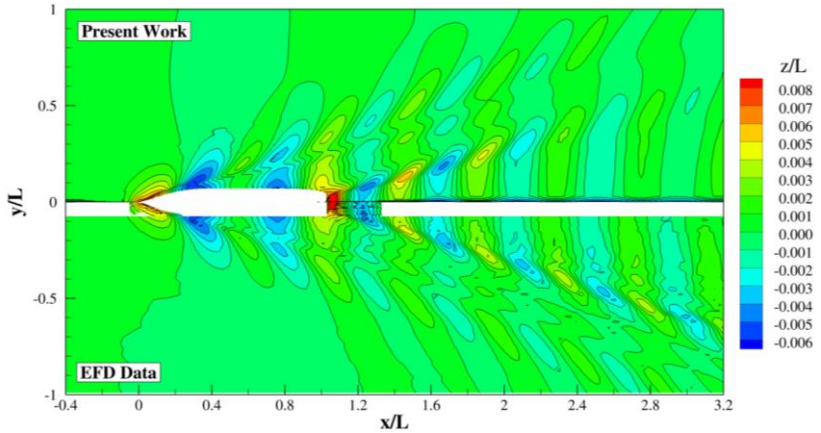

Figure 4: Wave pattern comparison between present work and EFD at Fr=0.26

5 SIMULATION RESULTS AND ANALYSIS

5.1 Resistance under different speeds

Figure 5 shows the trends of resistance coefficient under different speeds. The coefficient of viscous resistance C_v is relatively stable whereas the pressure resistance coefficient generally shows an increasing trend and hence the total resistance coefficient C_t maintain the same growth trend as C_p. At low speeds, C_v dominates and is around 80% of C_t at Fr=0.26. As the speed increases, the ship wave is gradually becoming apparent, and C_p begins to occupy a dominant position and is around 60% of C_t. In present study, the trend of resistance is consistent with the general consensus of ship hydrodynamics and the overall results show the feasibility of the current numerical method at both low speeds and high speeds.

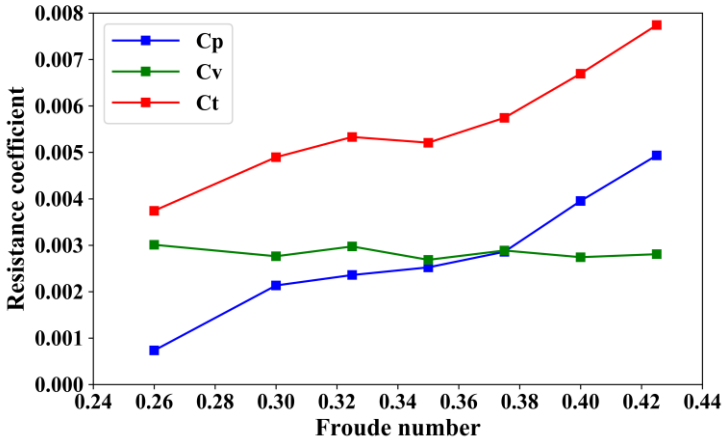

Figure 5: Resistance coefficient trends under different speeds

5.2 Wave profile on hull surface under different speeds

Figure 6 shows the wave profile on ship surface under different speeds. As the picture shows, the ship bow is always at the wave crest whereas the stern is at the trough. There are two crests and two troughs in each Froude number. The first crest appears at around x/L=0.1 and the maximum wave height (z/L=0.025) obtained when Fr=0.425 where Fr=0.26 gets the minimum wave height (z/L=0.01). The magnitude of second crest is smaller compared with the first crest and the position is around x/L=0.06. However, the maximum wave height is at Fr=0.30 with the value of z/L=0 and the minimum wave height appears when Fr=0.425 and the value is z/L=-0.01. The value difference of wave trough is smaller in contrast with the crest and the position is relatively dispersive. In this study, our focus is on the wave pattern and breaking near the bow which is primarily related to the first wave peak, hence the wave profiles of hull surface help us figure out the bow wave breaking region and wave performance under different speeds.

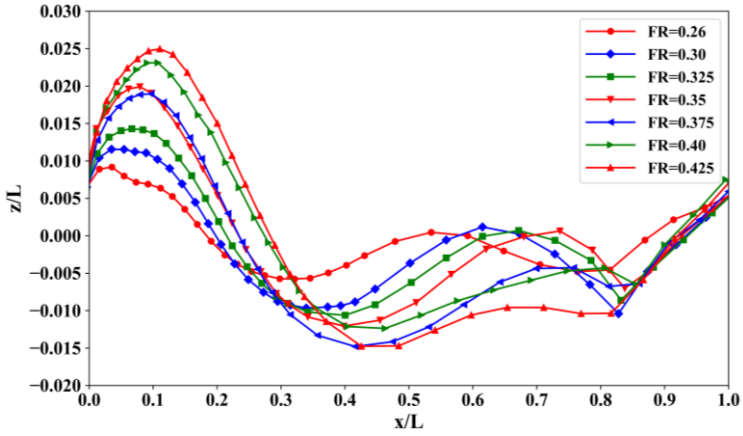

Figure 6: Wave profile on hull surface under different speeds

5.3 Bow wave breaking

In order to further verify the feasibility and credibility of current numerical methods in simulating wave breaking, three sets of comparison are shown in Figure 7 when Fr = 0.26, 0.35 and 0.425, respectively. At Fr=0.26, the bow wave is quite steady both in the CFD (Figure 7(a) and 7(b)) and EFD (Figure 7(c)), the overturning of bow wave can be found but the reconnect of free surface does not appear in this situation. As the speed increases and Fr=0.35, obvious bow wave breaking can be seen both in Figure 7(d), Figure 7(e) and Figure 7(f). One evident scar on account of the reconnection of free surface are developed along the x-axis in the bow wave region. At Fr=0.425 (Figure 7(g), Figure 7(h) Figure 7(i)), the wave performance shows the same trend as Fr=0.35 but more violent and two scars can be found in CFD study where only one scar is recognized in photo study of model test. Because of the unsteady capillary wave, it is hard to recognize the details of this region through photo study and present RANS model cannot capture this phenomenon.

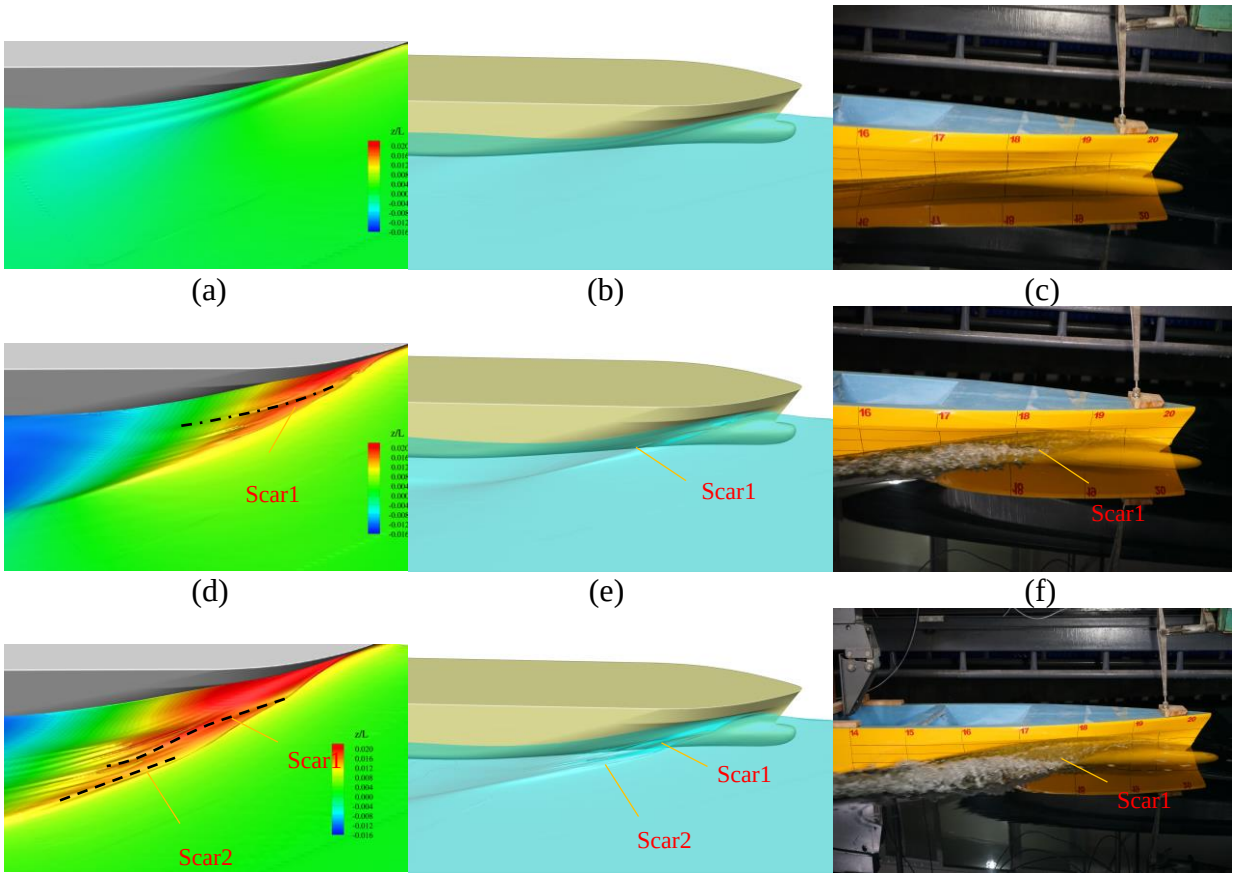

(a) (b) (c)

(d) (e) (f)

(g) (h) (i)

Figure 7: The comparison of bow wave breaking between CFD (the first two on the left) and EFD (right)
((a), (b), (c): Fr=0.26;
(d), (e), (f): Fr=0.35; (g), (h), (i): Fr=0.425)

According to the literatures, the spilling wave-breaking is usually without the overturning and air entrainment [13] where the plunging wave-breaking can be divided into three sub-procedures: jet impact, oblique splash and vertical jet [4]. Figure 8 shows the transverse cuts of wave pattern dyed by axial vorticity under different speeds and negative and positive vorticities corresponding to clockwise (CW) and counter-clockwise (CCW) rotations. According to Olivieri et al [5], the evolution of wave breaking is often accompanied by counter-rotating vortices. At Fr=0.26 (Figure 8(a)), the phenomenon of counter rotating is not obvious and the region of vorticity is quite close to the ship hull. At Fr=0.35 (Figure 8(b)), the vortex area has increased and counter-rotating vortices are generated around breaking region. The first couple of counter-rotating vortices (V1 and V2) are due to the plunging wave-breaking where the second couple (V3 and V4) and the third couple (V5 and V6) of vortices are generated by spilling wave-breaking. At Fr=0.425, two couple of counter-rotating vortices (V1 and V2, V3 and V4) associated with plunging breaking are generated and one couple (V5 and V6) of vortices are related to the spilling breaking. In order to figure out the mechanism of bow wave breaking, the case of Fr=0.35 is chosen for detail analysis.

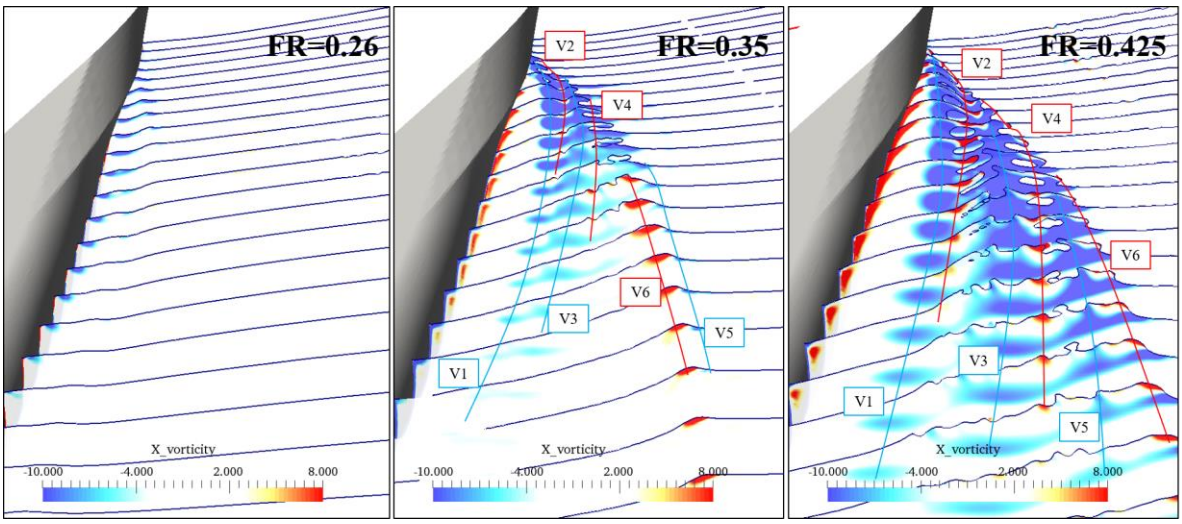

(a) (b) (c)

Figure 8: Transverse sections of wave cuts (black lines) and axial vorticity contours are shown in blue (CW) and red (CCW) at different Froude numbers: (a) Fr=0.26, (b) Fr=0.35, (c) Fr=0.425

Figure 9 and Figure 10 show the wave cuts along x-axis and y-axis at Fr=0.35 and the breaking type is plunging. The overall results show that the plunge is at an angle to the incoming flow, the overturning develops along the positive direction of the y-axis but the negative direction of the x-axis. Previous study about two-dimensional wave breaking always lay stress on evolution of wave breaking in the time domain. However, the study of three-dimensional breaker of ship wave should pay more attention to the evolution in the spatial domain.

The origin of plunging is around x/L=0.05 (Figure 9(a)) and y/L=0.025 (Figure 10(a)), a steep slope (the first jet) is generated. Reconnection of free surface and air entertainment can be recognized in Figure 9(b), Figure9(c), Figure 10(b) and Figure 10(c). Oblique splash is produced at the toe of the wave breaking and scar on account of the reconnection can be found before the toe. Figure 9(b) and Figure 10(b) show the first plunge where the second jet is distinct in Figure 9(c) and Figure 10(c). In Figure 9(d) and Figure 10(d), the first plunge is finished but the second jet dose not reconnect with the free surface and the breaking is much like spilling type. Away from the bow, the wave becomes steady in Figure 9(e), Figure 9(f), Figure 10(e) and Figure 10(f), small jets are generated.

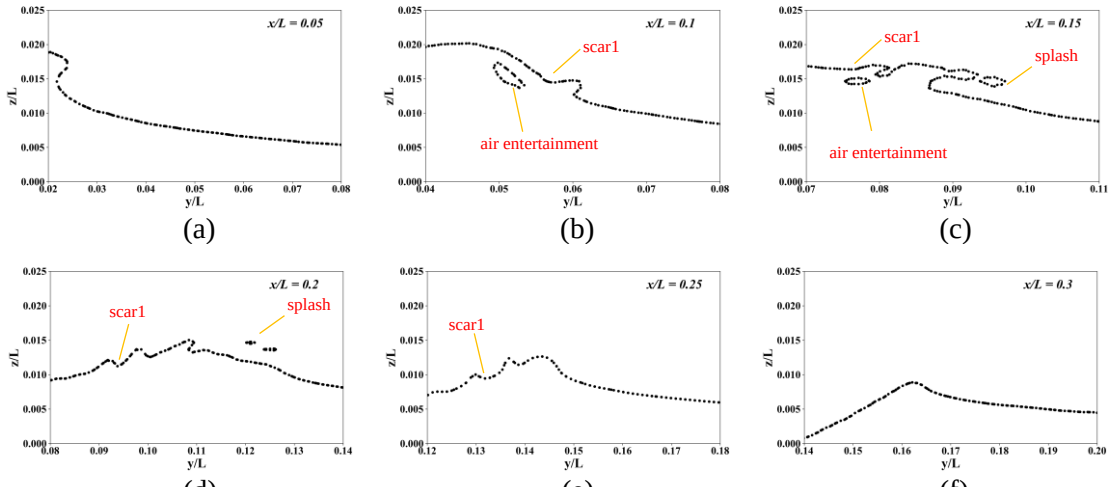

(a) (b) (c)

(d) (e) (f)

Figure 9: Wave cuts along the x-axis: (a) x/L=0.05, (b) x/L=0.1, (c) x/L=0.15, (d) x/L=0.2, (e) x/L=0.25, (f) x/L = 0.3

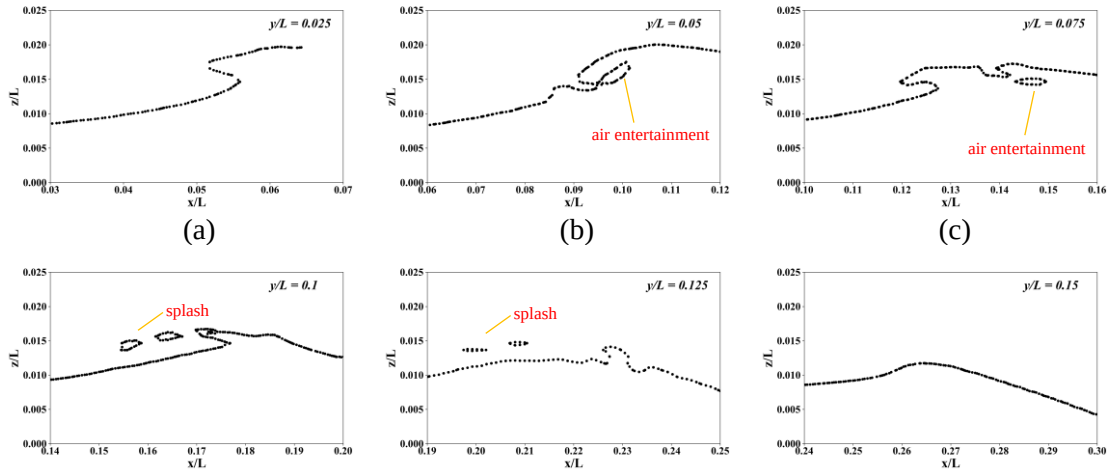

Figure 10: Wave cuts along the y-axis: (a) y/L=0.025, (b) y/L=0.05, (c) y/L=0.075, (d) y/L=0.1, (e) y/L=0.125, (f) y/L = 0.15

6 CONCLUSION

Present work mainly focuses on the bow wave breaking of a 6m-long KCS model and all the simulations are conducted by CFD solver naoe-FOAM-SJTU. RANS model is used to deal with the flow around ship where VOF method is employed to capture the air-water interface. The total resistance coefficient and wave pattern at Fr=0.26 are used for validation, the results show that present CFD method can accurately resolve the complex flow around KCS model. The trends of resistance coefficient and wave profile under seven Froude numbers (Fr=0.26, 0.30, 0.325, 0.35, 0.375, 0.40, 0.425) are provided. The trend of resistance coefficient is consistent with the general consensus of ship hydrodynamics and the wave profile of hull surface help us figure out the wave performance as well as bow wave regions. Three sets of comparison between CFD and EFD are shown with the Froude number of 0.26, 0.35 and 0.425. The simulation results show good agreement with model test and the overturning of bow wave is accurately captured. Besides, the vorticities induced by bow wave are also visualized and distinct counter-rotating vortices are recognized at Fr=0.35 and Fr=0.425. However, it is hard to recognize the details of the unsteady capillary wave region through photo study and present RANS model cannot capture this phenomenon. In order to figure out the mechanism of bow wave breaking, the wave cuts along x-axis and y-axis are provided at Fr=0.35. The overturning, air-entertainment and splash associated with plunging wave breaking can be recognized and the jet impact related to the spilling wave breaking is also found.

Future work will lay stress on the influence of different mesh distribution and turbulence model on the bow wave breaking. Detail analysis of vorticity, velocity and small scale characters will be carried out. Besides, more information will be measured in the model test and used for detailed CFD validation.

ACKNOWLEDGEMENTS

This work is supported by the National Natural Science Foundation of China (51879159, 51490675, 11432009, 51579145), Chang Jiang Scholars Program (T2014099), Shanghai Excellent Academic Leaders Program (17XD1402300), Program for Professor of Special Appointment (Eastern Scholar) at Shanghai Institutions of Higher Learning (2013022), Innovative Special Project of Numerical Tank of Ministry of Industry and Information Technology of China (2016-23/09) and Lloyd's Register Foundation for doctoral student, to which the authors are most grateful.

REFERENCES

[1] Baba, E. "A New Component of Viscous Resistance of Ships". *Journal of the Society of Naval Architects of Japan*, 125(1969), 23-34.

[2] Duncan, J.H. “The breaking and non-breaking wave resistance of a two-dimensional hydrofoil”. *Journal of Fluid Mechanics*, 126(1983), 507-520.

[3] Dong, R. R, Katz, J and T. T, Huang. “On the structure of waves on a ship model”. *J. Fluid Mech*, 346(1997), 77-115.

[4] Kang, D, Ghosh, S, Reins, G, Koo, B, Wang, Z. Y and F. Stern. “Impulsive plunging wave breaking downstream of a bump in a shallow water flume—Part I: Experimental observations”. *Journal of Fluids and Structures*, 32(20012), 104-120.

[5] Olivieri, A, Wilson, R, Campana, E. F and F. Stern. “Scars and Vortices Induced by Ship Bow and Shoulder Wave Breaking”. *Journal of Fluids Engineering*, 129(2007), 1444-1459.

[6] Rhee, S. H and F. Stern. “RANS Model for Spilling Breaking Waves”. *Transactions of ASME*, 124(2002), 424-432.

[7] Wilson, R. V, Carrica, P. M and F. Stern. “Simulation of ship breaking bow waves and induced vortices and scars”. *International journal for Numerical Methods in Fluids*, 54(2007), 419-451.

[8] Wang, J. H and Wan, D.C. “Breaking Wave Simulations of High-speed Surface Combatant using OpenFOAM”. In: *Proceedings of the 8th International Conference On Computational Methods (ICCM2017)*, Guiling, Guangxi, China, 2017.

[9] Ren, Z, Wang, J. H and Wan, D.C. “Numerical Simulations of Ship Bow and Shoulder Wave Breaking under Different Speeds”. In: *Proceedings of the 37th International Conference on Ocean, Offshore & Arctic Engineering (OMAE2018)*, Madrid, Spain, 2018.

[10] Shen, Z, Wan, D.C., and P. M. Carrica. “Dynamic overset grids in OpenFOAM with application to KCS self-propulsion and maneuvering”. *Ocean Eng*, 108(2015), 287–306.

[11] Marrone, S, Colagrossi, A, Antuono, M, Lugni, C and M.P. Tulin. “A 2D+t SPH model to study the breaking wave pattern generated by fast ships”. *Journal of Fluids & Structures*, 27(8)(2011), 1199-1215.

[12] Marrone, S, Bouscasse B, Colagrossi A and M. Antuono. “Study of ship wave breaking patterns using 3D parallel SPH simulations”. *Computer & Fluids*, 69(2012), 54-66.

[13] Deike, L, Popinet, S and W. K. Melville. “Capillary effects on wave breaking”. *J. Fluid Mech*, 769(2015), 541-569.